

Faraday instability threshold in large-aspect-ratio containers

By FRANCISCO J. MANCEBO AND JOSÉ M. VEGA

ETSI Aeronáuticos, Universidad Politécnica de Madrid, Plaza Cardenal Cisneros, 3,
28040 Madrid, Spain

We consider the Floquet linear problem giving the threshold acceleration for the appearance of Faraday waves in large-aspect-ratio containers, without further restrictions on the values of the parameters. We classify all distinguished limits for varying values of the various parameters and simplify the exact problem in each limit. The resulting simplified problems either admit closed-form solutions or are solved numerically by the well-known method introduced by Kumar & Tuckerman (1994). Some comparisons are made with (a) the numerical solution of the original exact problem, (b) some *ad hoc* approximations in the literature, and (c) some experimental results.

1. Introduction and formulation

Faraday waves (Faraday 1831) are gravity capillary waves excited parametrically by vertical vibration of the container. In addition to their intrinsic interest in fluid mechanics, these waves are considered today a prototype of a pattern forming system. The most interesting spatio-temporal behaviours are associated with nonlinearity (Miles & Henderson 1990; Fauve 1995), especially in large-aspect-ratio containers (Kudrolli & Gollub 1996), but unfortunately a complete, consistent weakly nonlinear theory for these waves is still lacking today, and some gaps still remain at the linear level. Among the still unresolved questions, linear damping is not completely understood for low viscosity at moderate aspect ratio, even if the effects of contact line dynamics and surface contamination are eliminated (Henderson & Miles 1994; Martel, Nicolás & Vega 1998; Howell *et al.* 2000). The theoretical and experimental determination of the instability threshold has received considerable attention, both in the moderate (Henderson & Miles 1990; Jiang *et al.* 1996) and large (Douady 1990; Edwards & Fauve 1994; Kumar & Tuckerman 1994; Bechhoefer *et al.* 1995; Christiansen, Alstrom & Levinsen 1995; Kumar 1996; Lioubashevski, Fineberg & Tuckerman 1997) aspect-ratio limits. In particular, if lateral walls are ignored the instability threshold is reliably calculated for arbitrary viscosity by a numerically cheap method (Kumar & Tuckerman 1994). But even in this simple case, a systematic asymptotic analysis of the several distinguished limits or regimes, to identify the relevant non-dimensional parameters in each case, is lacking. That analysis is the main object of this paper.

In order to formulate the problem we consider a wide cylindrical container, which is vertically vibrated with an amplitude a^* and frequency ω^* . We attach the reference frame to the container (figure 1) and non-dimensionalize space and time with the unperturbed height of the liquid h and the gravity-capillary time

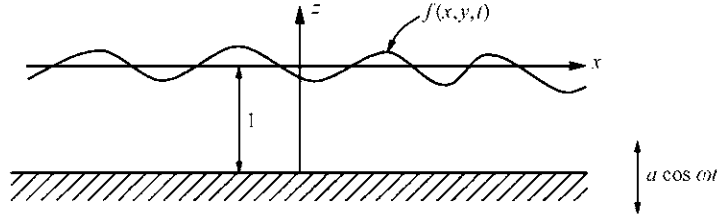


FIGURE 1. Sketch of the fluid domain.

$t_{cg}^* = [g/h + \sigma/(\rho h^3)]^{-1/2}$, where g is the gravitational acceleration and σ is the coefficient of surface tension. In addition, we linearize both the momentum equation and the boundary conditions around the quiescent state, to obtain

$$\nabla \cdot \mathbf{u} + w_z = 0, \quad (1.1)$$

$$\mathbf{u}_t = -\nabla p + C_g(\Delta \mathbf{u} + \mathbf{u}_{zz}), \quad w_t = -p_z + C_g(\Delta w + w_{zz}), \quad (1.2)$$

$$\mathbf{u} = \mathbf{0}, \quad w = 0 \quad \text{at } z = -1 \quad \text{and at } (x, y) \text{ in } \Gamma, \quad (1.3)$$

$$w = f, \quad \mathbf{u}_z + \nabla w = \mathbf{0} \quad \text{at } z = 0, \quad (1.4)$$

$$p - (1 - S)f + S\Delta f - 2C_g w_z + a\omega^2 f \cos(\omega t) = 0 \quad \text{at } z = 0, \quad (1.5)$$

$$f = 0 \quad \text{or} \quad f_t = D\nabla f \cdot \mathbf{n} \quad \text{at } \Gamma, \quad (1.6)$$

$$\int_{\Sigma} f \, dx \, dy = 0 \quad \text{at } t = 0, \quad (1.7)$$

where the boundary condition (1.6) depends on the attachment mode of the contact line (either pinned end or dynamical contact angle, with D a phenomenological constant, see Hocking 1987; Henderson & Miles 1994 and references therein). In the above equations \mathbf{u} and w are the horizontal and vertical components of the velocity, p is the pressure, f is the vertical deflection of the free surface, ∇ , $\nabla \cdot$ and Δ are the horizontal gradient, divergence and Laplacian operators, and Σ is the cross-section of the container; Γ is the boundary of Σ and the vector \mathbf{n} is the (horizontal) outward unit normal to Γ . The system is vibrating harmonically, with non-dimensional amplitude $a = a^*/h$ and frequency $\omega = 2\pi\omega^*t_{cg}^*$. In addition, the problem depends on the *capillary gravity number* $C_g = \nu/[gh^3 + \sigma h/\rho]^{1/2}$ and the *gravity capillary balance parameter* $S = \sigma/(\sigma + \rho gh^2)$, where ρ is the density and ν is the kinematic viscosity. C_g is the ratio of the capillary-gravity time to the viscous time, and is small most frequently in practice. C_g and S are related to the Ohnesorge number $C = \nu[\rho/\sigma h]^{1/2}$ and the Bond number $B = \rho gh^2/\sigma$ as $C_g = C/(1+B)^{1/2}$ and $S = 1/(1+B)$. Thus $0 \leq S \leq 1$, and the extreme values $S = 0$ and 1 correspond to the purely gravitational ($\sigma = 0$) and the purely capillary ($g = 0$) limits, respectively.

If the wavelength is sufficiently small compared to the aspect ratio (see § 5 below), we may ignore the lateral walls and reduce the stability problem (1.1)–(1.5) to the analysis of its normal modes, which are of the form

$$(\mathbf{u}, w, p, f) = (\mathbf{U}, W, P, F) \exp[i(k_1 x + k_2 y)], \quad (1.8)$$

in terms of the horizontal wavevector components k_1 and k_2 . Substitution of these expressions into (1.1)–(1.5) and elimination of \mathbf{U} yields

$$P_{zz} = k^2 P, \quad W_t = -P_z + C_g(W_{zz} - k^2 W), \quad (1.9)$$

$$W = W_z = 0 \quad \text{at } z = -1, \quad (1.10)$$

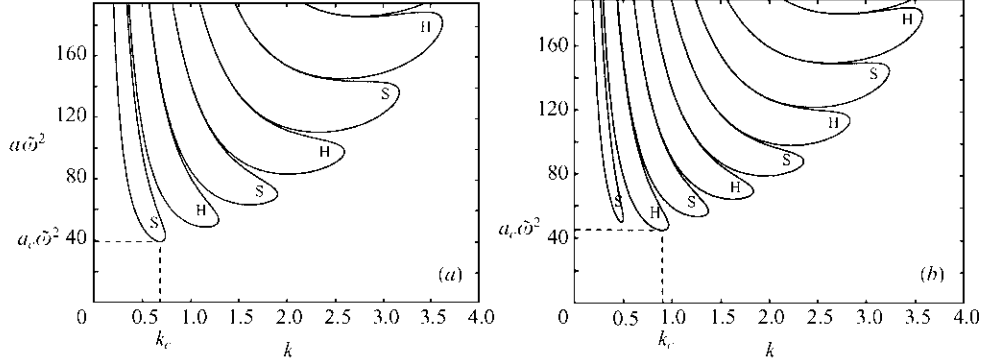


FIGURE 2. Representative neutral instability curves of (2.3)–(2.6) associated with sub-harmonic (S) and harmonic (H) perturbations. $C_g = 1$, $S = 0.5$ and (a) $\tilde{\omega} = 2$, (b) $\tilde{\omega} = 1.5$.

$$W - F_t = W_{zz} + k^2 W = 0 \quad \text{at } z = 0, \quad (1.11)$$

$$P - (1 - S + S k^2) F - 2 C_g W_z + a \omega^2 F \cos(\omega t) = 0 \quad \text{at } z = 0, \quad (1.12)$$

where $k = \sqrt{k_1^2 + k_2^2}$ is the wavenumber of the mode. The calculation of the *instability threshold* a_c requires determination those Floquet exponents of (1.9)–(1.12) that are purely imaginary; in fact, in all cases considered in this paper these exponents are found to be either 0 or $i\pi$, which correspond to real Floquet multipliers 1 or -1 respectively. For fixed values of the remaining parameters, this determines a sequence of tongues like that in figure 2, whose minimum yields a_c ; this is so because the flat solution is stable at $a = 0$. Using the method introduced by Kumar & Tuckerman (1994), the numerical calculation of the Floquet exponents is fairly cheap, even for extreme values of the parameters (see the Appendix). But, without further simplifications, a_c depends on three parameters: ω , C_g and S . Fortunately, these are usually large/small, and the number of parameters can be reduced under appropriate re-scaling and/or asymptotic analysis. We shall be mainly concerned with the distinguished limits, namely those limits in which the equations include as many terms as possible once a basic assumption is made. These limits are:

A. Nearly inviscid limits. If

$$C_g \ll 1, \quad C_g \ll 1 - S + \omega \quad \text{and} \quad C_g^{1/2} \omega^{3/2} \ll 1 - S + S\omega/C_g, \quad (1.13)$$

then the most dangerous mode at threshold is potential, except in two thin boundary layers near the bottom wall and the free surface, and an approximation of a_c can be found in closed form. As in the viscous limit below, several sub-limits can be distinguished, depending on the ratio of the container depth to the wavelength of the eigenmodes, and on whether the eigenmodes are monochromatic in first approximation or not.

B. Viscous limits. If (1.13) does not hold, then the most dangerous mode at threshold exhibits non-localized vorticity due to viscous effects. Two sub-limits are considered, depending on which condition (1.13) fails.

B.1. Moderate and long waves. Now the most dangerous mode at threshold exhibits a bounded wavenumber and thus it affects the whole fluid field, down to the bottom of the container. We shall consider three cases.

B.1.1. Basic limit and highly viscous sub-limit. This is the most general limit, which is captured as

$$C_g^{-1} = O(1) \quad \text{and} \quad \omega \sim C_g, \quad (1.14)$$

and includes as sub-limits the remaining limits considered below. As usual, O denotes hereinafter the Landau O -symbol, namely $\psi = O(\phi)$ means that either $\psi \ll \phi$ or $\psi \sim \phi$. If (1.14) holds with $C_g \gg 1$ then viscous effects dominate gravity and surface tension, which can both be ignored in (1.12).

B.1.2. Long-wave limit. This limit applies if $C_g \ll 1$ and (1.13b) fails, namely if

$$C_g \ll 1, \quad 1 - S = O(C_g) \quad \text{and} \quad \omega = O(C_g). \quad (1.15)$$

The wavenumber of the most dangerous mode is small and we can neglect those terms proportional to k^2 in (1.9) and (1.11), and neglect the term proportional to C_g in (1.12).

B.1.3. Small-frequency limit. This is a sub-limit of the limits *A*, *B.1.1* and *B.1.2*, and applies when

$$C_g^{-1} = O(1) \quad \text{and} \quad \omega \ll C_g, \quad \text{or} \quad C_g \ll 1, \quad 1 - S = O(C_g) \quad \text{and} \quad \omega \ll C_g. \quad (1.16)$$

The most dangerous mode at threshold oscillates on a time scale much shorter than ω^{-1} and can be calculated by a WKB approximation.

B.2. Short waves. This limit applies when the wavelength of the most dangerous mode is small compared to depth. It occurs when either $C_g \ll 1$ and (1.13c) fails, or C_g is at least of order unity and $\omega \gg C_g$, namely

$$C_g \ll 1 \quad \text{and} \quad 1 - S + S\omega/C_g = O(C_g^{1/2}\omega^{3/2}), \quad \text{or} \quad \omega^{-1} \ll C_g^{-1} = O(1). \quad (1.17)$$

Now the most dangerous mode at threshold only affects a thin layer of thickness $O(k^{-1})$ near the free surface.

Note that if (1.13) does not hold then one of the conditions (1.14)–(1.17) holds. Thus the classification above covers all possible values of the parameters, including some that are somewhat unlikely in practice but are also considered for the sake of completeness.

With these ideas in mind, the paper is organized as follows. The viscous and nearly inviscid limits will be analysed in §2 and §3, respectively. The results of this analysis will be compared in §4 with some previous approximations in the literature. The effect of distant sidewalls and a comparison with experimental results in the literature will be made in §5 and §6 respectively. Some concluding remarks will be made in §7.

2. Viscous limits

These limits apply if (1.13) does not hold.

2.1. Moderate and long waves

Now the wavelength of the most dangerous mode at threshold is either of the order of the height of the container or larger. Three distinguished limits are considered.

2.1.1. Basic limit and highly viscous sub-limit

Let us assume that

$$\omega^{-1} \sim C_g^{-1} = O(1), \quad (2.1)$$

with S arbitrary. This is the most general limit and leads to no simplification in (1.9)–(1.12). For convenience we introduce the re-scaling

$$\tilde{P} = P/C_g, \quad \tilde{F} = C_g F, \quad \tilde{t} = C_g t, \quad \tilde{\omega} = \omega/C_g, \quad (2.2)$$

which corresponds to non-dimensionalizing time with the viscous time h^2/ν . Equations (1.9)–(1.12) are rewritten as

$$\tilde{P}_{zz} = k^2 \tilde{P}, \quad \tilde{W}_{\tilde{t}} = -\tilde{P}_z + W_{zz} - k^2 W, \quad (2.3)$$

$$W = W_z = 0 \quad \text{at} \quad z = -1, \quad (2.4)$$

$$W - \tilde{F}_{\tilde{t}} = W_{zz} + k^2 W = 0, \quad (2.5)$$

$$\tilde{P} - (1 - S + Sk^2)\tilde{F}/C_g^2 - 2W_z + a\tilde{\omega}^2\tilde{F} \cos(\tilde{\omega}\tilde{t}) = 0 \quad \text{at} \quad z = 0. \quad (2.6)$$

For fixed values of C_g , $\tilde{\omega}$ and S , this problem can be solved as indicated in the Appendix, to obtain marginal instability curves for harmonic and sub-harmonic perturbations (1 and -1 Floquet multipliers) that are like the resonance tongues in figure 2, where the minimum is indicated and provides the threshold amplitude, which corresponds to a sub-harmonic perturbation for $\tilde{\omega} = 2$ and to a harmonic one for $\tilde{\omega} = 1.5$. When $\tilde{\omega}$ is varied, the solid curves in figure 3 are obtained. As $C_g \rightarrow \infty$ the instability threshold becomes independent of both gravity and surface tension (see (2.6)). Thus the curve labelled $C_g = \infty$ in figure 3(d) is independent of S ; this curve gives a quite good approximation for C_g only moderately large (e.g. for $C_g = 2$ the curve would be indistinguishable from that for $C_g = \infty$). Note that for $\tilde{\omega} > \tilde{\omega}_0$ (~ 2 if $C_g \geq 0.5$) the threshold a_c is attained at the first (from the left) resonance tongue in figure 2, which corresponds to a sub-harmonic instability. And as ω is decreased the whole group of resonance tongues in figure 2 rolls clockwise (in addition to moving up) in such a way that the minimum changes to a higher-order tongue, and the instability alternately changes from sub-harmonic to harmonic and vice versa (at the points indicated with circles in figure 3). As $\tilde{\omega} \rightarrow 0$ the eigenmodes exhibit oscillations on the time scale $\tilde{t} \sim 1$ but a much larger period, of the order of $\tilde{\omega}^{-1}$; in this limit the curves (a), (c) and (d) in figure 3 match with the asymptotic results in §2.1.3 obtained by the WKB method and

$$a_c \tilde{\omega}^2 \rightarrow \tilde{A}_c \quad \text{as} \quad \tilde{\omega} \rightarrow 0, \quad (2.7)$$

where the constant \tilde{A}_c is plotted vs. S (for the indicated values of C_g) in figure 5(b) below. On the other hand we have the asymptotic behaviour, which is obtained below in §2.2;

$$a_c \tilde{\omega}^{1/2} \rightarrow \tilde{A}_{c,2} \simeq 1.672 \quad \text{as} \quad \tilde{\omega} \rightarrow \infty. \quad (2.8)$$

2.1.2. Long-wave limit

Now the wavelength of the most dangerous mode is small, and requires that viscosity, gravity and the forcing frequency be correspondingly small, namely

$$C_g \ll 1, \quad 1 - S = O(C_g) \quad \text{and} \quad \omega = O(C_g). \quad (2.9)$$

The distinguished limit is $1 - S \sim k^2 \sim \omega \sim a^{-1} \sim C_g \ll 1$, and leads to the scaling

$$\left. \begin{aligned} \tilde{P}_1 &= (1 - S + C_g)P, & \tilde{W} &= C_g W, & \tilde{F}_1 &= C_g^2 F, \\ \tilde{k} &= k/(1 - S + C_g)^{1/2}, & \gamma &= (1 - S)/C_g, & \tilde{a} &= C_g a, \end{aligned} \right\} \quad (2.10)$$

with $\tilde{t} = C_g t$ and $\tilde{\omega} = \omega/C_g$ as in §2.1.1, and to the following approximation of (1.9)–(1.12):

$$\tilde{P}_1 = \text{constant}, \quad \tilde{W}_{\tilde{t}} = -\tilde{k}^2 \tilde{P}_1 + \tilde{W}_{zzz}, \quad (2.11)$$

$$\tilde{W} = \tilde{W}_z = 0 \quad \text{at} \quad z = -1, \quad (2.12)$$

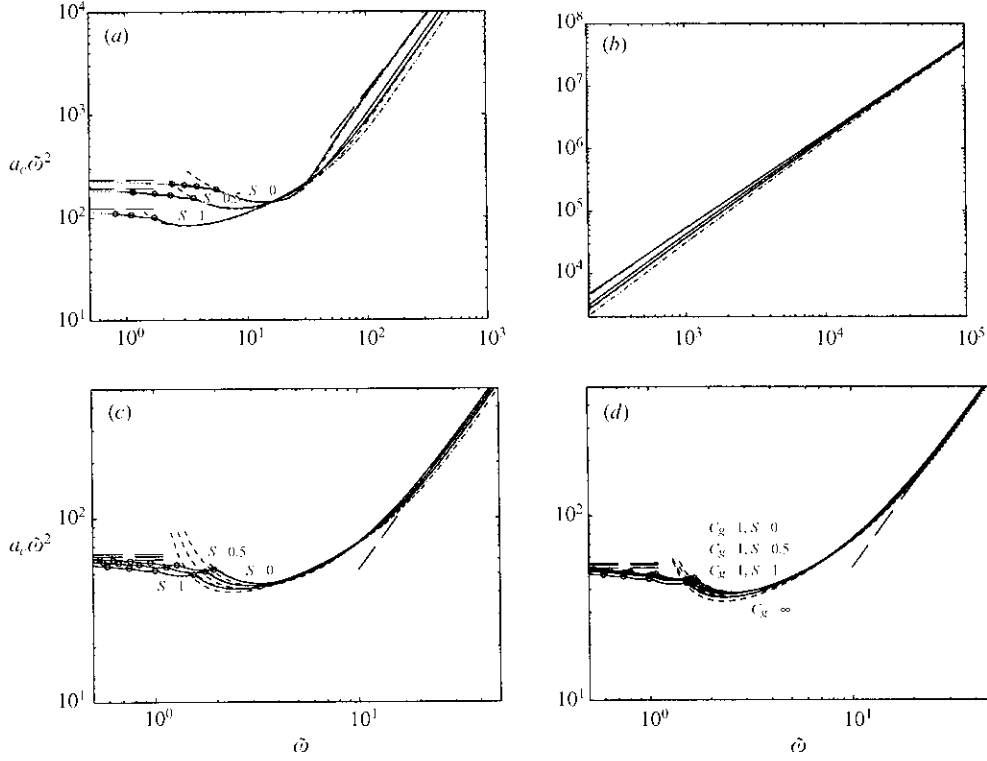


FIGURE 3. Basic and highly viscous limits. Instability threshold acceleration of (2.3)–(2.6), $a_c \tilde{\omega}^2 \equiv a_c^* h^3 (2\pi\omega^*)^2 / \nu^2$ in terms of $\tilde{\omega} \equiv 2\pi\omega^* h^2 / \nu$, for (a, b) $C_g = 0.1$, (c) $C_g = 0.5$, (d) $C_g = 1, \infty$, and the indicated values of S . Exact (—), two-term approximation in (A 9) (---), Cerda & Tirapegui (1998) approximation (- · - · -), WKB approximation from the Mathieu equation (4.3) (·····), and asymptotic behaviours as $\tilde{\omega} \rightarrow 0, \infty$ (—).

$$\tilde{W} - \tilde{F}_{1f} = \tilde{W}_{zz} = \tilde{P}_1 / (\gamma + 1) - [\gamma + (\gamma + 1)\tilde{k}^2 - \tilde{a}\tilde{\omega}^2 \cos \tilde{\omega}\tilde{t}] \tilde{F}_1 = 0 \quad \text{at } z = 0. \quad (2.13)$$

This problem depends on \tilde{k} , $\tilde{\omega}$, \tilde{a} and γ and, when solved as indicated in the Appendix, provides the instability threshold $\tilde{a}_c \tilde{\omega}^2$ plotted vs. $\tilde{\omega}$ in figure 4 for several representative values of γ . As in §2.1.1, the instability is sub-harmonic for sufficiently large $\tilde{\omega}$ and changes alternately from sub-harmonic to harmonic and vice versa (at the points indicated with circles) as $\tilde{\omega}$ is decreased. The asymptotic behaviours

$$\tilde{a}_c \tilde{\omega}^2 \rightarrow \tilde{A}_{c1} \quad \text{as } \tilde{\omega} \rightarrow 0 \quad \text{and} \quad \tilde{a}_c \tilde{\omega}^{3/2} \rightarrow 1 \quad \text{as } \tilde{\omega} \rightarrow \infty \quad (2.14)$$

are plotted with dashed lines, as obtained in §2.2 and §3.1 below; $\tilde{A}_{c1}/(\gamma + 1)$ is plotted vs. $\gamma/(\gamma + 1)$ in figure 5(d) below.

2.1.3. Small-frequency limit

This limit applies whenever the forcing frequency is sufficiently small. It is a sub-limit of the limits considered above, in §2.1.1 and §2.1.2, and applies when either

$$C_g^{-1} = O(1) \quad \text{and} \quad \omega \ll C_g, \quad (2.15)$$

or

$$1 - S = O(C_g) \quad \text{and} \quad \omega \ll C_g \ll 1. \quad (2.16)$$

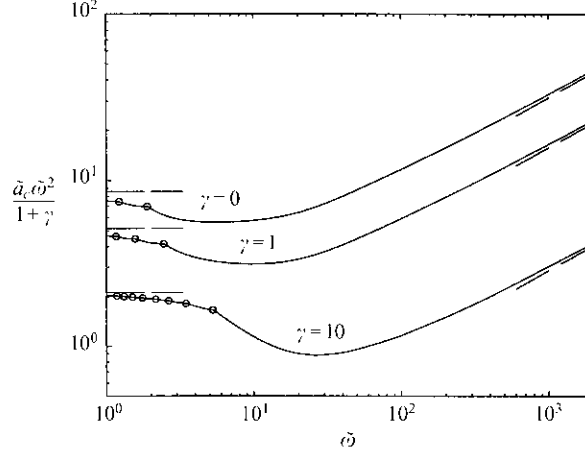


FIGURE 4. Viscous long-wave limit. Instability threshold acceleration of (2.11)–(2.13), $\tilde{a}_c \tilde{\omega}^2 \equiv a_c^*(2\pi\omega^*)^2 h^3 / [\nu(gh^3 + \sigma h/\rho)^{1/2}]$ in terms of $\tilde{\omega} \equiv 2\pi\omega^* h^2/\nu$, for the indicated values of $\gamma \equiv gh^3 / [\nu(gh^3 + \sigma h/\rho)^{1/2}]$.

In the limit (2.15) we apply a WKB approximation. We re-scale \tilde{t} and a as

$$\tau = \tilde{\omega} \tilde{t}, \quad \tilde{A} = a \tilde{\omega}^2, \quad (2.17)$$

where $\tilde{\omega} = \omega/C_g$ as above, and then seek solutions of (2.3)–(2.6) of the form

$$(W, \tilde{P}, \tilde{F}) = (W_0(z, \tau), \tilde{P}_0(z, \tau), \tilde{F}_0(\tau)) \exp \left[\tilde{\omega}^{-1} \int_0^\tau \tilde{\lambda}(\sigma) d\sigma \right] + \text{c.c.} + \dots \quad (2.18)$$

as $\tilde{\omega} \rightarrow 0$, where c.c. stands for the complex conjugate. When this ansatz and (2.17) are placed into (2.3)–(2.6) and higher-order terms are neglected, we obtain

$$\tilde{P}_{0zz} = k^2 \tilde{P}_0, \quad \tilde{\lambda} W_0 = -\tilde{P}_{0z} + W_{0zz} - k^2 W_0, \quad (2.19)$$

$$W_0 = W_{0z} = 0 \quad \text{at } z = -1, \quad (2.20)$$

$$W_0 - \tilde{\lambda} \tilde{F}_0 = W_{0zz} + k^2 W_0 = 0 \quad \text{at } z = 0, \quad (2.21)$$

$$\tilde{P}_0 - (1 - S + Sk^2) \tilde{F}_0 / C_g^2 + \tilde{A} \tilde{F}_0 \cos \tau - 2W_{0z} = 0 \quad \text{at } z = 0, \quad (2.22)$$

where the slow time variable τ acts as a parameter and $\tilde{\lambda}(\tau)$ is defined as that eigenvalue with largest real part; this is numerically calculated from the dispersion relation of (2.19)–(2.22), which is $A_0(\tilde{\lambda}, \tau) = 0$, where A_0 is the right-hand side of (A 3) in the Appendix, after setting $n = 0$ and subtracting $\tilde{A} \cos \tau$. As usual in the WKB method (Bender & Orszag 1978; Wasow 1987), the associated approximation of the time derivatives breaks down at the turning points, which correspond to the multiple eigenvalues of (2.19)–(2.22); but this failure does not affect our leading-order approximation. Now, according to (2.18), the marginally unstable points are given by

$$\text{Re} \left(\int_0^{2\pi} \tilde{\lambda}(\tau) d\tau \right) = 0, \quad (2.23)$$

where Re stands for the real part. This equation provides the marginal instability value of \tilde{A} , which is shown as a thick line in figure 5(a). For comparison, the exact marginal instability curves for $\tilde{\omega} = 0.3$ are also plotted. Note that the approximation is reasonably good near the minimum, even for this not-so-small value of $\tilde{\omega}$, but it

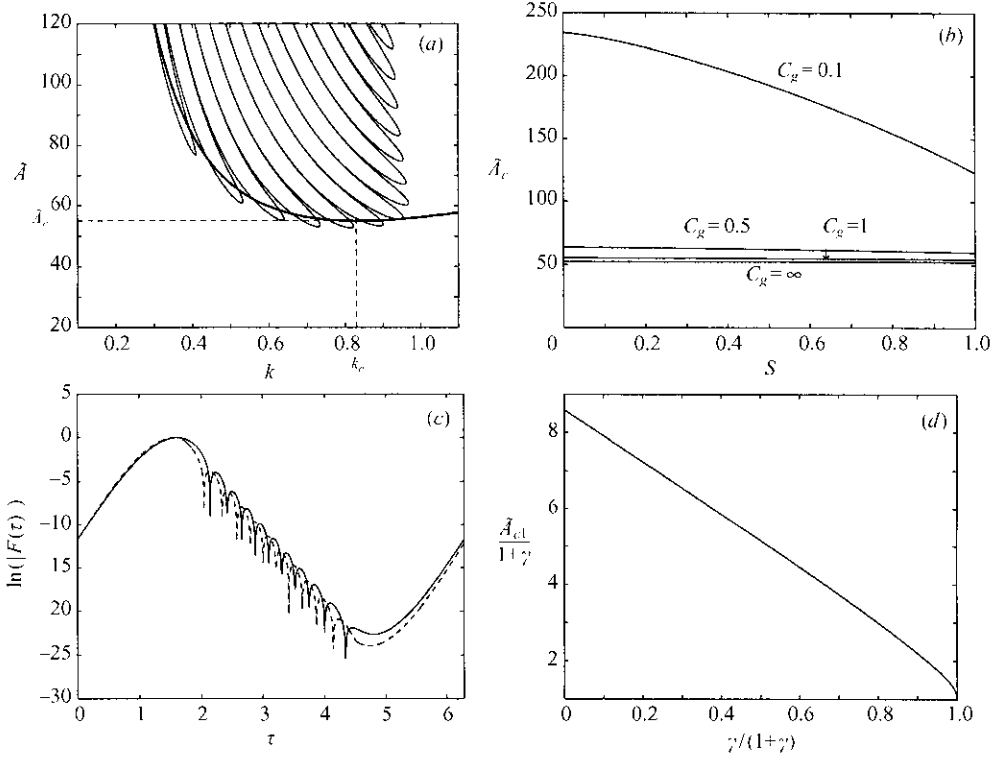


FIGURE 5. Small-frequency sub-limit. (a) Marginal instability curve for $C_g = 1$, $S = 0.5$; asymptotic results as $\tilde{\omega} \rightarrow 0$ calculated from (2.23) (thick line) and exact results calculated from (2.3)–(2.6) for $\tilde{\omega} = 0.3$ (thin lines). (b) Asymptotic (as $\tilde{\omega} \rightarrow 0$) instability threshold acceleration in terms of S , as calculated from (2.23) for the indicated values of C_g . (c) Asymptotic (as $\tilde{\omega} \rightarrow 0$) (---) and exact (—) eigenfunction for $k_c = 0.83$, $C_g = 1$, $S = 0.5$, $A_c = 55$. (d) Asymptotic (as $\tilde{\omega} \rightarrow 0$) threshold acceleration in the long-wave limit (2.11)–(2.13).

does not distinguish between harmonic and sub-harmonic perturbations; this would require consideration of higher-order terms and analysis of the turning points. The instability threshold acceleration \tilde{A}_c is readily obtained as that value of \tilde{A} where the plot in figure 5(a) attains its minimum, at $k = k_c \simeq 0.83$. For other parameter values we obtain \tilde{A}_c in terms of C_g and S , as plotted in figure 5(b). The corresponding eigenfunction $\tilde{F}(\tau) = \tilde{F}_0(\tau) \exp[\tilde{\omega}^{-1} \int_0^\tau \tilde{\lambda}(\sigma) d\sigma] + \text{c.c.}$ (see (2.18)) at threshold, $k = k_c$, is plotted in figure 5(c), and compared with the exact eigenfunction at $\tilde{\omega} = 0.3$; once again the comparison is reasonably good.

In the limit (2.16) we must consider the WKB approximation of (2.11)–(2.13) as $\tilde{\omega} \rightarrow 0$. As above, the instability threshold in this limit is obtained from equation (2.23), where $\tilde{\lambda}(\tau)$ is that eigenvalue with largest real part of the problem obtained by substituting $\tau = \tilde{\omega}\tilde{t}$, $\tilde{A} = \tilde{a}\tilde{\omega}^2$ and $(W, P, \tilde{F}) = (W_0(z, \tau), P_0(z, \tau), \tilde{F}_0(\tau)) \exp[\tilde{\omega}^{-1} \int_0^\tau \tilde{\lambda}(\sigma) d\sigma] + \text{c.c.} + \dots$ in (2.11)–(2.13), and neglecting higher-order terms as $\tilde{\omega} \rightarrow 0$. For the sake of brevity we do not give explicitly here this linear eigenvalue problem, but it yields

$$\tilde{a}_c \tilde{\omega}^2 \rightarrow \tilde{A}_{c1} \quad \text{as } \tilde{\omega} \rightarrow 0, \quad (2.24)$$

where the constant $\tilde{A}_{c1}/(\gamma + 1)$ is plotted vs. $\gamma/(\gamma + 1)$ in figure 5(d).

2.2. Short waves

This limit applies when either

$$C_g^{-1} = O(1) \quad \text{and} \quad \omega \gg C_g, \quad (2.25)$$

or

$$C_g \ll 1 \quad \text{and} \quad \omega \gg 1. \quad (2.26)$$

Under either of these conditions, the most dangerous wavenumber is large and the associated eigenmode is such that the velocity vanishes except in a thin layer attached to the free surface, whose thickness is of the order of the wavelength (i.e. small as compared to the height of the container, which is 1).

If (2.25) holds then the distinguished limit is

$$\omega \sim k^2 \sim a^{-2} \gg 1, \quad C_g \sim 1. \quad (2.27)$$

Using the scaling

$$\left. \begin{aligned} \hat{P} &= C_g^{-1/2} \omega^{-1/2} P, & \hat{F} &= \omega F, & \eta &= C_g^{-1/2} \omega^{1/2} z, & \tau &= \omega t, \\ \hat{k} &= C_g^{1/2} \omega^{-1/2} k, & \hat{A} &= C_g^{-1/2} \omega^{1/2} a, \end{aligned} \right\} \quad (2.28)$$

(1.10)–(1.12) are rewritten in this layer as

$$\hat{P}_{\eta\eta} = \hat{k}^2 \hat{P}, \quad W_\tau = -\hat{P}_\eta + W_{\eta\eta} - \hat{k}^2 W, \quad (2.29)$$

$$W = 0 \quad \text{at} \quad \eta = -\infty, \quad (2.30)$$

$$W - \hat{F}_\tau = W_{\eta\eta} + \hat{k}^2 W = 0 \quad \text{at} \quad \eta = 0, \quad (2.31)$$

$$\hat{P} - 2W_\eta + \hat{A}\hat{F} \cos \tau = 0 \quad \text{at} \quad \eta = 0. \quad (2.32)$$

Note that this problem is independent of both gravity and surface tension, which are dominated in (2.32) by viscous effects. Thus this limit can also be obtained as a sub-limit (as $\tilde{\omega} \rightarrow \infty$) of the highly viscous limit considered in §2.1.1. The problem depends only on \hat{k} and \hat{A} , and when solved as indicated in the Appendix yields the instability threshold $\hat{A}_c = \hat{A}_{c2} \simeq 1.672$, which provides the asymptotic behaviour (2.8).

If (2.26) holds then the distinguished limit is

$$\omega^2 \sim k \sim C_g^{2/3} \sim S^{-1/2} \sim a^{-1} \gg 1 \quad (2.33)$$

and leads to the scaling defined by (2.28) and

$$\hat{\omega} = C_g^3 \omega / (S + C_g^{4/3})^2, \quad \hat{S} = C_g^{4/3} S. \quad (2.34)$$

Using these, (1.9)–(1.11) are rewritten as given by (2.29)–(2.31), and (1.12) becomes

$$\hat{P} - [(1 + \hat{S})^{-3} \hat{\omega}^{-3/2} + (1 + \hat{S})^{-1} \hat{\omega}^{-1/2} \hat{S} \hat{k}^2] \hat{F} - 2W_\eta + \hat{A}\hat{F} \cos \tau = 0 \quad \text{at} \quad \eta = 0. \quad (2.35)$$

As above, this problem is solved numerically (see the Appendix) to obtain the Faraday stability threshold acceleration \hat{A}_c plotted vs. $\hat{\omega}$ in figure 6(a). Note that as $\hat{\omega}$ increases all curves approach that labelled $\hat{S} = \infty$, which corresponds to neglecting gravity and replacing (2.35) by

$$\hat{P} - \hat{\omega}^{-1/2} \hat{k}^2 \hat{F} - 2W_\eta + \hat{A}\hat{F} \cos \tau = 0 \quad \text{at} \quad \eta = 0. \quad (2.36)$$

Now, we must distinguish two cases. (i) If $\hat{S} = O(1)$ the validity of (2.36) requires that

$$(1 + \hat{S})^3 \hat{\omega}^{3/2} \equiv C_g^{1/2} \omega^{3/2} \gg 1, \quad (2.37)$$

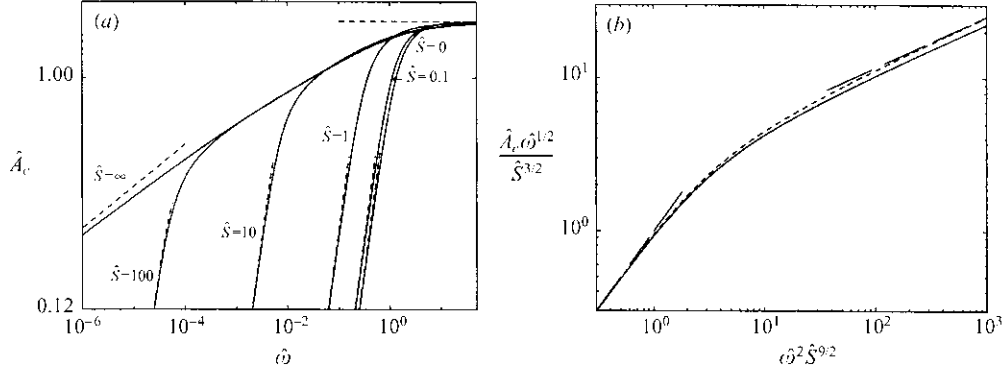


FIGURE 6. Short-wave limit. (a) Instability threshold of (2.29)–(2.31) and (2.35), given by $\hat{A}_c \equiv a_c^*(2\pi\omega^*/v)^{1/2}$ in terms of $\hat{\omega} \equiv 2\pi\omega^*\rho^2v^3/[\sigma + (\rho v^2)^{2/3}(\rho g + \sigma/h^2)^{1/3}]^2$, for the indicated values of $\hat{S} \equiv \sigma/[(\rho v^2)^{2/3}(\rho g + \sigma/h^2)^{1/3}]$; asymptotic behaviours as $\hat{\omega} \rightarrow 0, \infty$ (---). (b) Comparison between the approximation (2.39) (or (3.20)), giving $\hat{A}_c \hat{\omega}^{1/2} \hat{S}^{3/2} \equiv a_c \omega S^{1/2}/C_g$ in terms of $\hat{\omega}^2 \hat{S}^{9/2} \equiv \omega^2 S^{1/2}$ (---) and the exact threshold acceleration calculated from (2.29)–(2.31) and (2.35) for $\hat{S} = 500$ (—); asymptotic behaviours as $\hat{\omega}^2 \hat{S}^{9/2} \rightarrow 0, \infty$ (---).

as obtained by comparing those terms accounting for gravitational and viscous effects in (2.35). Similarly, capillary effects are small compared to viscous effects provided that

$$(1 + \hat{S})\hat{\omega}^{1/2}/\hat{S} \equiv C_g^{3/2}\omega^{1/2}/S \gg 1. \quad (2.38)$$

(ii) If instead $\hat{S} \gg 1$ then gravity can be neglected for $\hat{\omega} \ll 1$. In this limit, (3.19) below holds, the short-wave limit of the nearly inviscid regime (§ 3.1.1 below) applies, and according to (3.20) below and the scaling (2.34), the threshold curve is given by

$$\hat{\omega}^2 \hat{S}^{9/2} = \hat{\omega}^{1/2} \hat{S}^{3/2} \hat{A}_c [1 + (\hat{\omega}^{1/2} \hat{S}^{3/2} \hat{A}_c)^2/16], \quad (2.39)$$

to a first approximation; in fact this approximation applies whenever $\hat{\omega} \ll 1$, without the need for \hat{S} being large. This approximate expression is plotted in figure 6(b), where it is also compared with the ‘exact’ curve for $\hat{S} = 500$, and yields two asymptotic behaviours, as $\hat{\omega}^2 \hat{S}^{9/2} \ll 1$ and as $\hat{\omega}^2 \hat{S}^{9/2} \gg 1$, which become apparent in the curve labelled $\hat{S} = 100$ in figure 6(a).

The asymptotic behaviours as $\hat{\omega} \rightarrow 0$ and $\hat{\omega} \rightarrow \infty$ are also plotted in figure 6(a). According to our comments above, the former is given by

$$\hat{A}_c = 2(4\hat{\omega})^{1/6} + \dots \quad \text{if } \hat{S} = \infty, \quad \hat{A}_c = \hat{S}^3 \hat{\omega}^{3/2} + \dots \quad \text{if } \hat{S} < \infty. \quad (2.40)$$

In the limit $\hat{\omega} \rightarrow \infty$, when both (2.37) and (2.38) hold, (2.35) reduces to (2.32) and thus we have the asymptotic behaviour $\hat{A}_c \rightarrow \hat{A}_{c2} (\simeq 1.672)$ as $\hat{\omega} \rightarrow \infty$, which coincides with both the asymptotic behaviour (2.8) and the related result above in the limit (2.25).

3. Nearly inviscid limits

In these limits viscous effects can be ignored except in two boundary layers attached to the bottom wall and the free surface. This requires that (see below)

$$C_g \ll 1, \quad C_g \ll 1 - S + \omega \quad \text{and} \quad C_g^{1/2} \omega^{3/2} \ll 1 - S + S\omega/C_g. \quad (3.1)$$

If we tried to obtain the whole marginal instability curve in this regime then we would obtain a non-local Mathieu equation similar to those considered by Beycr & Friedrich (1995) and Müller *et al.* (1997). But for most values of the parameters in this regime, namely whenever (cf. (3.1))

$$C_g \ll 1, \quad C_g \ll \omega \quad \text{and} \quad C_g^{1/2} \omega^{3/2} \ll 1 - S + S\omega/C_g, \quad (3.2)$$

the eigenfunction at threshold is monochromatic to a first approximation and the instability threshold is given by a standard Mathieu equation. This case will be treated in §3.1. If instead (3.1) holds but (3.2) does not, which occurs if

$$C_g \ll 1, \quad \omega = O(C_g) \quad \text{and} \quad C_g \ll 1 - S, \quad (3.3)$$

then the eigenfunction at threshold is not monochromatic but the WKB method applies.

3.1. Monochromatic eigenfunctions

In the limit (3.2) the free-surface deflection F is given by

$$F'' + 2\delta F' + [\Omega^2 - 2\Omega d + 2d^2 - ak\omega^2 \tanh k \cos(\omega t)]F = 0, \quad (3.4)$$

where the damping rate δ , the inviscid eigenfrequency Ω and the viscous detuning d are

$$\delta = \frac{k(\Omega/2)^{1/2}}{\sinh 2k} C_g^{1/2} + \left[2k^2 + \frac{(1 + \tanh^2 k)k^2}{4 \sinh^2 k} \right] C_g + \dots, \quad (3.5)$$

$$\Omega = [k \tanh k (1 - S + Sk^2)]^{1/2}, \quad d = \frac{k(\Omega/2)^{1/2}}{\sinh 2k} C_g^{1/2} + \dots. \quad (3.6)$$

Note that the second term in the expansion (3.5) is essential as soon as k is large. The two-term approximation of the damping rate (3.5) is quite good in the whole range (3.2) (Martel & Knobloch 1997). Note that there is a discrepancy between the coefficient of C_g in (3.5) and its counterpart calculated by Martel & Knobloch, which comes from a gap in their calculation (Knobloch, Martel & Vega 2002). But this term can be in fact neglected, to obtain the following well-known approximation:

$$\delta \simeq k[(1 - S + Sk^2)k \tanh k]^{1/4} C_g^{1/2} / (2^{1/2} \sinh 2k) + 2k^2 C_g, \quad (3.7)$$

which is uniformly valid in the limit (3.2). Of course we could proceed with higher-order terms in (3.5), but their calculation is increasingly tedious and only provides small corrections (the next $O(C_g^{3/2})$ -term yields a 15% correction at $C_g \simeq 0.1$, Müller *et al.* 1997). Equation (3.4) could be obtained quite directly by adding viscous dissipation to the standard inviscid Mathieu equation (Kumar & Tuckerman 1994). But for convenience we explain how (3.4) (with δ approximated as in (3.7)) is derived from first principles and where its validity limits (3.2) come from. We consider the distinguished limit $C_g \ll 1$, $\omega \sim 1$, in which the solutions of (1.9)–(1.12) exhibit two thin boundary layers, with thicknesses $O(C_g^{1/2})$, near the bottom plate and the free surface. Outside these layers, in the bulk, (1.9)–(1.12) can be replaced by

$$P_{zz} = k^2 P, \quad W_t = -P_z, \quad (3.8)$$

$$W = [C_g/(2\Omega)]^{1/2} (W_{zt}/\Omega - W_z) \quad \text{at} \quad z = -1, \quad (3.9)$$

$$W - F_t = -2k^2 C_g F \quad \text{at} \quad z = 0, \quad (3.10)$$

$$P - (1 - S + Sk^2)F - 2C_g W_z + a\omega^2 F \cos(\omega t) = 0 \quad \text{at} \quad z = 0, \quad (3.11)$$

to the approximation relevant here, where we have taken into account that vorticity vanishes to all orders in the bulk; the boundary conditions are obtained from matching conditions between the solution in the boundary layers and that in the bulk. The assumption above that the solution be monochromatic is essential to obtain the solution in the boundary layer attached to the bottom plate in closed form.

Since $C_g \ll 1$, we seek the expansions

$$(P, W) = (P_0, W_0) + C_g^{1/2}(P_1, W_1) + C_g(P_2, W_2) + \dots, \quad (3.12)$$

and introduce the ansatz

$$F'' = -[\mathcal{L}_0(F) + C_g^{1/2}\mathcal{L}_1(F) + C_g\mathcal{L}_2(F) + \dots], \quad (3.13)$$

where, for $j = 0, 1, 2$, \mathcal{L}_j are linear operators acting on the free-surface deflection F . Substituting (3.12)–(3.13) into (3.8)–(3.11) we obtain, at leading order,

$$\left. \begin{aligned} W_0 = F' \sinh[k(z+1)]/\sinh k, \quad P_0 = -F'' \cosh[k(z+1)]/(k \sinh k), \\ \mathcal{L}_0(F) = k \tanh k [1 - S + Sk^2 - a\omega^2 \cos(\omega t)]F, \end{aligned} \right\} \quad (3.14)$$

where the third expression comes from a standard solvability condition. Similarly, at $O(C_g^{1/2})$ and $O(C_g)$ we obtain

$$\left. \begin{aligned} \mathcal{L}_1(F) = k(2\Omega)^{1/2}(F' - \Omega F)/\sinh 2k, \\ \mathcal{L}_2(F) = 4k^2 F' + O(k^2 F' + d^2 F)/\sinh^2 k \end{aligned} \right\} \quad (3.15)$$

and, according to (3.13), the Mathieu equation (3.4) follows. When looking at the ingredients in this derivation, we obtain the validity limits (3.2) by anticipating that $\omega \sim \Omega$ and requiring that the thicknesses of the boundary layers, $O(C_g/\omega)^{1/2}$, be small compared to either (i) the height of the container if ω is bounded or (ii) the penetration depth of the waves, k^{-1} , if ω is large.

Now since $\delta \ll 1$, the stability analysis of (3.4) is standard. The most dangerous mode is the sub-harmonic (and monochromatic, as anticipated above) one with a frequency $\Omega \simeq \omega/2$, which corresponds to a first resonance tongue and gives $a_c \sim \delta$; the remaining tongues are associated with modes exhibiting frequencies $m\omega/2$ and yield $a \sim \delta^{1/m}$ ($\gg \delta$) for each integer $m \geq 2$ (Bender & Orszag 1978), and thus they never provide the instability threshold. For fixed values of ω , C_g ($\ll 1$) and S , the first resonance tongue corresponds to values of the wavenumber k such that $\Omega(k)$ is close to $\omega/2$, and the marginal instability curve (a vs. k) of (3.4) is given by

$$(\omega k \tanh k)a/\delta = 2[1 + (\Omega - \omega/2 - d)^2/\delta^2]^{1/2} \quad (3.16)$$

to the approximation relevant here. As the wavelength is (slightly) varied, this condition provides the hyperbola plotted as a solid line in figure 7(a), whose minimum is attained at $\Omega = \omega/2 + d$ and leads to the threshold amplitude for Faraday instability, which is

$$a_c = 2\delta/(\omega k \tanh k) \simeq (\coth^2 k - 1)C_g^{1/2}/(2\omega^{1/2}) + 4k \coth k C_g/\omega, \quad (3.17)$$

where the approximation (3.7) has been used and the wavenumber k is given by (recall that $\Omega \simeq \omega/2$ and see (3.6a))

$$(1 - S + Sk^2)k \tanh k = \omega^2/4. \quad (3.18)$$

The approximation (3.17) is plotted with dashed lines in figure 7(b, c) for $C_g = 10^{-2}$. Note that the approximation is good provided that ω is neither too small nor too large,

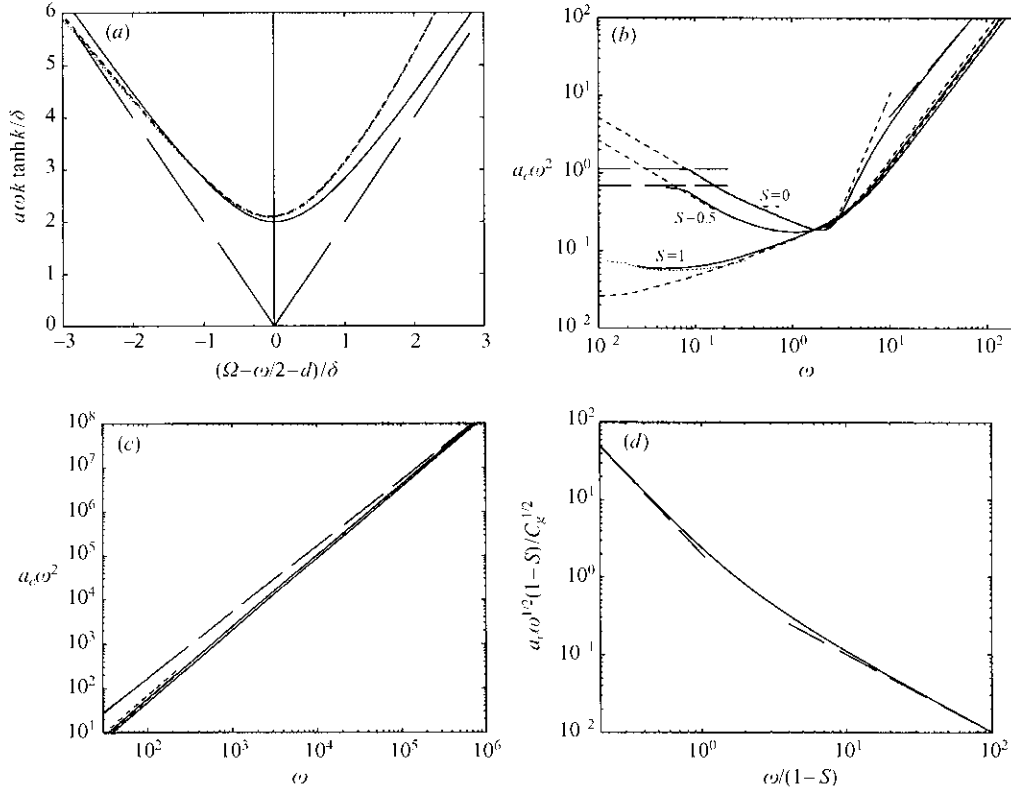


FIGURE 7. Instability threshold in the nearly inviscid regime. (a) Marginal instability curves; asymptotic result from (3.16) (—), and exact result from (1.9)–(1.12) for $C_g = 10^{-2}$, $\omega = 1$ and: $S = 0$ (---), $S = 0.5$ (- · - · -) and $S = 1$ (· · · · ·). (b, c) Instability threshold acceleration in terms of ω for the indicated values of S ; asymptotic result from (3.17) (---), exact result from (1.9)–(1.12) for $C_g = 10^{-2}$ (—); asymptotic behaviours from (3.20) and (3.24) (—), and long-wave approximation from (2.11) (2.13) (· · · · ·). (d) Approximation (3.23) (—) and asymptotic behaviours for small and large $\omega/(1-S)$ (—).

according to (3.2). In addition, the exact value of a_c and its asymptotic behaviour (as $\omega \rightarrow 0$ and $\omega \rightarrow \infty$) are plotted for comparison. These asymptotic behaviours deserve some attention.

Nearly inviscid short waves

If

$$1 \ll \omega \quad \text{and} \quad C_g^{1/2} \omega^{3/2} \ll 1 - S + S\omega/C_g, \quad (3.19)$$

then k is large at threshold (see (3.18)) and (3.17)–(3.18) become $a_c = 4kC_g/\omega$ and $(1 - S + Sk^2)k = \omega^2/4$ to a first approximation, or

$$\omega^2 S^{1/2} = (\omega S^{1/2} a_c / C_g) [1 + (\omega S^{1/2} a_c / C_g)^2 / 16]. \quad (3.20)$$

This expression is readily obtained in the distinguished limit $Sk^2 \sim 1$ (which requires that S be small), but also applies as either $Sk^2 \rightarrow 0$ or $Sk^2 \rightarrow \infty$, as is readily seen. It matches with the short-wave limit considered in §2.2, as anticipated there.

Nearly inviscid long waves

If

$$C_g \ll \omega \ll 1, \quad (3.21)$$

then the wavenumber k is small (see (3.18)) and, to a first approximation, (3.17)–(3.18) become

$$a_c = C_g^{1/2}/(2\omega^{1/2}k^2) \quad \text{and} \quad (1 - S + Sk^2)k^2 = \omega^2/4, \quad (3.22)$$

which can be simplified to

$$a_c \omega^{1/2}(1 - S)/C_g^{1/2} = (1 - S)^2/\omega^2 + [(1 - S)^4/\omega^4 + (1 - S)^2/\omega^2]^{1/2}. \quad (3.23)$$

In order to obtain this we only need to consider the distinguished limit $1 - S \sim k^2$ (which requires that $1 - S$ be small) in (3.22) and check that the approximation also holds as $1 - S \ll k^2$ and as $1 - S \gg k^2$. This approximation yields the threshold curve plotted in figure 7(d), where the asymptotic behaviours are

$$a_c \omega^{3/2} C_g^{-1/2} \rightarrow 1 \quad \text{as} \quad \omega/(1 - S) \rightarrow \infty, \quad (3.24)$$

$$a_c \omega^{5/2} C_g^{-1/2} (1 - S)^{-1} \rightarrow 2 \quad \text{as} \quad \omega/(1 - S) \rightarrow 0. \quad (3.25)$$

Asymptotic behaviour (3.25) matches either with the long-wave limit considered in § 2.1.2 (see (2.14b)) if $1 - S = O(C_g)$, or with the non-monochromatic case considered next if $1 - S \gg C_g$.

3.2. Non-monochromatic eigenfunctions

In the limit (3.3) the eigenfunctions at threshold are not monochromatic and oscillate on a characteristic time much shorter than the forcing period $2\pi/\omega$. As in § 2.1.3, those eigenfunctions and the instability threshold are readily calculated by the WKB method, which in the limit (3.3) leads to closed-form expressions as follows. As in the approximation implicit in (3.6), (3.7), the eigenvalue of (2.19)–(2.22) is given by

$$\begin{aligned} C_g \tilde{\lambda}(\tau) = & [(a\omega^2 \cos \tau - 1 + S - Sk^2)k \tanh k]^{1/2} \\ & - [(a\omega^2 \cos \tau - 1 + S - Sk^2)k \tanh k]^{1/4} k C_g^{1/2} / (2^{1/2} \sinh 2k) - 2k^2 C_g + \dots \end{aligned} \quad (3.26)$$

which applies in the limit (3.3) provided that, in addition $\text{Im } \tilde{\lambda} \gg |\text{Re } \tilde{\lambda}|$, where Re and Im stand for the real and the imaginary parts. This requires in particular that $\tilde{\lambda}$ be not real. Thus invoking (2.23) and (3.26), and anticipating that $Sk^2 \ll 1$ at marginal instability we have

$$a\omega^2 = 1 - S + A, \quad \text{with} \quad |A| \ll 1, \quad (3.27)$$

we obtain the following approximation for A :

$$\begin{aligned} I_1(1 - S)^{-1/2}(A - Sk^2)(k \tanh k)^{1/2} \\ = I_2[(1 - S)k \tanh k]^{1/4} k C_g^{1/2} / [2 \sinh(2k)] + 4\pi k^2 C_g + \dots, \end{aligned} \quad (3.28)$$

where

$$\begin{aligned} I_1 &= \sqrt{2} \int_0^1 (1 - \xi^2)^{1/2} d\xi = \pi/2^{3/2} \\ I_2 &= \int_0^{2\pi} (1 - \cos \tau)^{1/4} d\tau = 2^{5/4} B(3/4, 1/2) \simeq 5.70, \end{aligned}$$

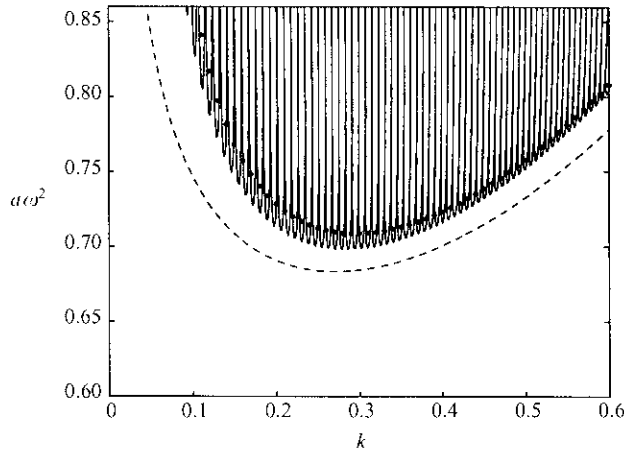


FIGURE 8. Marginal instability curves for $C_g = 10^{-2}$, $S = 0.5$ and $\omega = 0.01$: —, exact solution from (2.3)–(2.6); ---, approximate WKB solution given by (3.27)–(3.28) and ·····, approximate WKB solution as calculated in §2.1.3.

B being the beta-function (Abramowitz & Stegun 1972). Equations (3.27)–(3.28) yield a U-shaped curve, like that plotted with a dashed line in figure 8, whose minimum provides the instability threshold. The approximation (3.28) does not coincide, even at leading order, with the result of applying the WKB method (as $\omega \rightarrow 0$) to the Mathieu equation (3.5), the main difference being the term proportional to $C_g^{1/2} \cos \tau$ in (3.26); this is not surprising because (3.5) only applies when the oscillation is monochromatic.

4. Some approximations in the literature

Here we consider two *ad hoc* approximations already considered in the literature to elucidate their scope.

As noticed by Kumar (1996) and further pursued by Miles (1999), the numerical solution of the basic problem used by Kumar & Tuckerman (1994), quoted in the Appendix, converges so fast that a two-term truncation frequently yields quite good results. That approximation is given by (Λ 9) in the Appendix and has been used to calculate those curves plotted with dashed lines in figure 3. From this figure and other comparisons not presented here we conclude that the approximation is reasonably good along the first resonance tongue. Note that the eigenfunctions are increasingly complex as $\tilde{\omega} \rightarrow 0$ (§2.1.3) and thus this two-mode approximation must fail for small frequency. Also note that the approximation is better for small C_g , which is consistent with the fact that in the nearly inviscid limit the eigenfunctions become monochromatic.

A second (family of) approximation(s) is related to the Mathieu equation, which is the simplest equation exhibiting parametric instabilities (Bender & Orszag 1978). There has been two types of such approximations reported.

Beyer & Friedrich (1995) and Müller *et al.* (1997) derived a non-local Mathieu equation in the nearly inviscid limit $C_g \rightarrow 0$, the non-local term resulting from the solution in the Stokes boundary layer attached to the bottom of the container. That equation reduces to (3.4) if the forcing frequency is not too large and only monochromatic solutions are sought, but it also provides the non-monochromatic solutions considered in §3.2.

Cerda & Tirapegui (1998) instead considered the highly viscous limit and proceeded as follows. They considered the temporal Laplace transform of (2.3)–(2.6),

$$(\tilde{P}^*, W^*, \tilde{F}^*) = \int_0^{\infty} (\tilde{P}, W, \tilde{F}) e^{s\tilde{t}} d\tilde{t}, \quad (4.1)$$

and eliminated \tilde{P}^* and W^* from the resulting problem, to obtain after some algebra an equation of the form

$$\mathcal{P}(s)\tilde{F}^* + a\tilde{\omega}^2 \int_0^{\infty} \tilde{F}^* \cos(\tilde{\omega}\tilde{t}) e^{s\tilde{t}} d\tilde{t} = 0. \quad (4.2)$$

Now they observed that for sufficiently large viscosity and fixed forcing frequency (in our notation, $C_g \gg 1$ and ω fixed) the function \mathcal{P} is well-approximated by its second-order Taylor expansion at $s = 0$, namely $\mathcal{P}(s) \simeq \mathcal{P}(0) + s\mathcal{P}'(0) + s^2\mathcal{P}''(0)/2$ over a wide range in s (not just that at small s). This means that the inverse Laplace transform of (4.2) is approximated by a Mathieu equation. In our notation, this equation is

$$B_1(k)\tilde{F}'' + B_2(k)\tilde{F}' + [(1 - S + Sk^2)/C_g^2 + a\tilde{\omega}^2 \cos(\tilde{\omega}\tilde{t})]\tilde{F} = 0, \quad (4.3)$$

where

$$\left. \begin{aligned} B_1(k) &= (3 \sinh 2k - 6k - 4k^3) \cosh^2 k + k^2(\sinh 2k - 2k)/[k(\sinh 2k - 2k)^2], \\ B_2(k) &= 2k(\cosh k + 2k^2 + 1)/(\sinh 2k - 2k). \end{aligned} \right\} \quad (4.4)$$

Before proceeding we note that (4.3) does not reduce to (3.4) as $C_g \rightarrow 0$, which means that (4.3) does not apply as $\omega \gg C_g \rightarrow 0$. Observe that (4.3) does not come from any asymptotic limit; instead it should be seen as a numerical approximation. We have thoroughly checked (4.3) and have found that it provides (numerically) reasonably good results over a wide range of the parameter values, whenever $\tilde{\omega}$ is not too large. This is illustrated in figure 3. Finally, we can obtain a second-order approximation in the application of the WKB method to (4.3) (Bender & Orszag 1978), namely the following approximation of the marginal instability curve of (4.3):

$$\int_0^{2\pi} \operatorname{Re}(\tilde{\lambda}(\tau)) d\tau = -\tilde{\omega} \ln \left[2 \left| \cos \left(\tilde{\omega}^{-1} \int_0^{2\pi} \operatorname{Im}(\tilde{\lambda}(\tau)) d\tau \right) \right| \right] + \dots \quad (4.5)$$

as $\tilde{\omega} \rightarrow 0$, where $\tilde{\lambda}$ is that root of

$$B_1(k)\tilde{\lambda}^2 + B_2(k)\tilde{\lambda} + [(1 - S + Sk^2)/C_g^2 + a\tilde{\omega}^2 \cos(\tilde{\omega}\tilde{t})]\tilde{F} = 0, \quad (4.6)$$

with the largest real part. With this approximation we calculate the threshold acceleration that is plotted with dotted lines in figure 3.

Summarizing, the two-term approximation in (A 9) and that resulting from the Mathieu equation (4.3) together provide the whole threshold curve, as is apparent in figure 3.

5. The effect of distant sidewalls

These effects were neglected above, but they can be larger than expected due to contact line dynamics; they have been estimated at large aspect ratio by Milner (1991), and are considered below for convenience. In the viscous regime considered in §2, the validity of the approximation only requires that the aspect ratio of the

container, L (the ratio of width to depth), be large compared to the non-dimensional wavelength k , that is

$$Lk \gg 1. \quad (5.1)$$

And the same condition applies in the nearly inviscid limit considered in §2.1 if the contact line is either fixed or completely free (i.e. if either the first boundary condition (1.6) applies or if the second does with $D = \infty$); this is in accordance with the fact that the contact line itself produces no dissipation at leading order in these two cases. But if the second boundary condition (1.6) applies and D is neither too small nor too large, then contact line dynamics has a more profound effect on viscous dissipation and thus on the instability threshold calculated in §3, as we show now. With the notation in (1.1)–(1.6), the mechanical energy equation is written as

$$dH/dt = -\Phi_1 - \Phi_2 + \Phi_3,$$

where H , Φ_1 , Φ_2 and Φ_3 are given by

$$\begin{aligned} H &= \int_{\Sigma} \int_{-1}^0 (|\mathbf{u}|^2 + w^2) \, dx \, dy \, dz + \int_{\Sigma} [(1-S)f^2 + S|\nabla f|^2] \, dx \, dy, \\ \Phi_1 &= 2C_g \int_{\Sigma} \int_{-1}^0 (|\nabla \mathbf{u}|^2 + |\mathbf{u}_z|^2 + |\nabla w|^2 + w_z^2) \, dx \, dy \, dz + 4C_g \int_{\Sigma} \mathbf{u} \cdot \mathbf{u}_z \, dx \, dy, \\ \Phi_2 &= 2SD^{-1} \int_{\Gamma} f_t^2 \, ds = 2SD \int_{\Gamma} (\nabla f \cdot \mathbf{n})^2 \, ds, \quad \Phi_3 = 2a\omega^2 \cos \omega t \int_{\Sigma} f f_t \, dx \, dy. \end{aligned}$$

H and Φ_3 result from mechanical energy and the work due to forced vibration, respectively. Φ_1 accounts for viscous dissipation in the liquid, which results from dissipation in both the bulk and the Stokes boundary layer, and was accounted for in (3.5) (or (3.7)); Φ_2 comes from dissipation at the contact line. A straightforward orders-of-magnitude analysis using (3.12) and (3.14) yields

$$|\Phi_1| \sim C_g \omega^2 k^2 L^2 (1+k)^{-1} \quad \text{and} \quad |\Phi_2| \sim SL \min\{D^{-1}\omega^2, Dk^2\},$$

and the effect of viscous dissipation at the contact line can be neglected only if

$$\frac{|\Phi_2|}{|\Phi_1|} \sim \frac{S(1+k) \min\{1, D^2 k^2 / \omega^2\}}{C_g D k^2 L} \ll 1, \quad (5.2)$$

or equivalently, only if D is either sufficiently small or large, namely if either

$$D \ll \omega^2 C_g L / [S(1+k)] \quad \text{or} \quad D \gg S(1+k) / (C_g k^2 L).$$

If none of these conditions hold then the effect of contact line dynamics can be of the same order as (or even large compared to) that of viscous dissipation. This could be the case in some of the experiments by Bechhoefer *et al.* (1995) and Christiansen *et al.* (1995).

6. Comparison with experiments

Most experiments in large-aspect-ratio containers either deal with the viscous limit or with the short-wave limit, which are considered now.

6.1. Highly viscous limit

As is frequently the case in fluid mechanics, the high-viscosity limit provides good results for moderate viscosity. In order to illustrate this we plot in figure 9(a) the

Symbol in figure 9(b)	ρ (g cm ⁻³)	ν (cm ² s ⁻¹)	σ (dyn cm ⁻¹)	h (cm)	ω^* (Hz)	C_g	S
\triangle	0.8	0.8	30	0.13	40–80	0.30	0.69
\times	0.8	0.8	30	0.15	40–80	0.27	0.63
$+$	0.8	0.58	30	0.1	30–70	0.27	0.75

TABLE 1. Experiments at large viscosity by Lioubashevski *et al.* (1997).

threshold acceleration for representative values of $C_g \geq 0.3$ and S (cf. figure 3*c, d*). Note that for $C_g > 0.3$ and $\tilde{\omega} > 10$ (or $C_g > 0.5$ and $\tilde{\omega} > 5$), all curves are quite close to that obtained for $C_g = \infty$. This explains the ‘universal scaling’ found by Lioubashevski *et al.* (1997), who performed a large number of experiments at high viscosity and small depth, and showed that the results were fairly independent of gravity and surface tension. In our notation, these results were all on the same curve of the plane a_c vs. $\tilde{\omega}$, in accordance with figure 9(*a*). In fact, by empirical fit, Lioubashevski *et al.* obtained the curve

$$a_c \tilde{\omega}^2 = (\pi/2)[(1 - S)C_g^{-2} + 0.059 \tilde{\omega}^2 + 21.46 \tilde{\omega}^{0.23}], \quad (6.1)$$

which is plotted with dot-dashed line in figure 9(*a, b*). This curve yields reasonably good results in the range $5 < \tilde{\omega} < 10$, which (as it must) includes the range where it fitted the experiments by Lioubashevski *et al.* Note nevertheless that it cannot (and does not) give good results outside this range; in particular (as expected in a purely empirical fit) it does not meet the asymptotic behaviour (2.8) for large $\tilde{\omega}$. For illustration we have added in figure 9(*b*) some experimental results by Lioubashevski *et al.* (see table 1 for the physical parameters). Note that $C_g \sim 0.3$ and $S \sim 0.7$ in all cases, and that the fit is quite good with both the exact curves and the empirical approximation (6.1) for $C_g = 0.3$ and $S = 0.7$.

6.2. Short-wave limit

Now we consider the experimental results summarized in table 2. These are compared in figure 9(*c*) with the results obtained in §2.2. Note that condition (2.26) applies in all cases. Most results (except some by Hoffman & Wolf 1974 and Bechhoefer *et al.* 1995) fit the curve $\hat{S} = \infty$, which suggests that gravity plays no much role here. But a closer look at the theoretical curves for the different values of \hat{S} shows that the effect of gravity (and surface tension) is as indicated in the last column in table 2. Some remarks are now in order.

(i) The experimental points are above the theoretical curves in most plots, which suggests that (despite experimental errors) some additional source of damping could be present. The effect of the lower plate, which was ignored in the theoretical curves, could also play a minor role when ω is only moderately large (say $\omega \leq 6$).

(ii) Some of the second group of experimental points by Hoffman & Wolf (namely, those above the curve $\hat{S} = \infty$) were obtained with the container in the inverted position, which confirms the small role of gravity.

(iii) Kudrolli & Gollub (1996) do not give the surface tension coefficient, which has been taken from Bechhoefer *et al.* (1997), because both seem to have used the same type of silicone oil.

(iv) We have only taken a few from the many experimental points by Wernet *et al.* (2001), namely those points in which the wavelength of the excited waves was small

Experiment [symbol in figure 9c]	ρ (g cm ⁻³)	ν (cm ² s ⁻¹)	σ (dyn cm ⁻¹)	h (cm)	ω^* (Hz)	$C_g \times 10^3$	$S \times 10^3$	ω	\hat{S}	Dominant effects
Hoffman & Wolf (1974) [★]	0.9	1.1	10	6	50–170	2.4	0.31	25–84	1.00	V-S-G
Hoffman & Wolf (1974) [×]	0.9	4.3	10	6	50–110	9.4	0.31	25–55	0.16	V
Edwards (1994) [⊕]	1.22	1.02	67.6	0.29	51–100	160	400	4.3–8.4	4.58	V-S(-G)
Bechhoefer <i>et al.</i> (1995) [△]	0.86	1.24	28.9	1.0	30–75	39	33	6.0–15	2.46	V-S(-G)
Bechhoefer <i>et al.</i> (1995) [▽]	0.84	0.25	26.2	1.0	54–137	7.9	31	11–27	19.7	V-S-G
Kudrolli & Gollub (1996) [+]	0.85	0.1	27	0.3	42–178	16.6	265	3.9–16	62.6	V-S(-G)
Kudrolli & Gollub (1996) [□]	0.85	0.5	27	0.3	42–57	83	265	4.0–5.4	7.27	V-S(-G)
Kudrolli & Gollub (1996) [⊗]	0.85	1	27	0.3	47–58	166	265	4.5–5.3	2.90	V-S(-G)
Lioubashevski <i>et al.</i> (1997) [⊙]	0.8	0.48	30	0.21	66–80	117	465	4.5–5.3	8.16	V-S
Lioubashevski <i>et al.</i> (1997) [●]	0.8	0.41	30	0.25	52–102	82.5	380	4.1–8.1	10.6	V-S(-G)
Wernet <i>et al.</i> (2001) [◇]	~ 0.94	~ 0.75	~ 19.9	0.3	80–140	~ 140	~ 193	7.9–14	~ 2.7	V-S

TABLE 2. Experiments in deep containers. In the last column we indicate what effects (V = viscous, G = gravitational, S = surface tension) play a role in each experiment; G between parentheses indicates that gravity plays a small role. The data for Edwards (1994) are unpublished and are taken from Kumar & Tuckerman (1994), Kumar (1996) and Cerda & Tirapegui (1998).

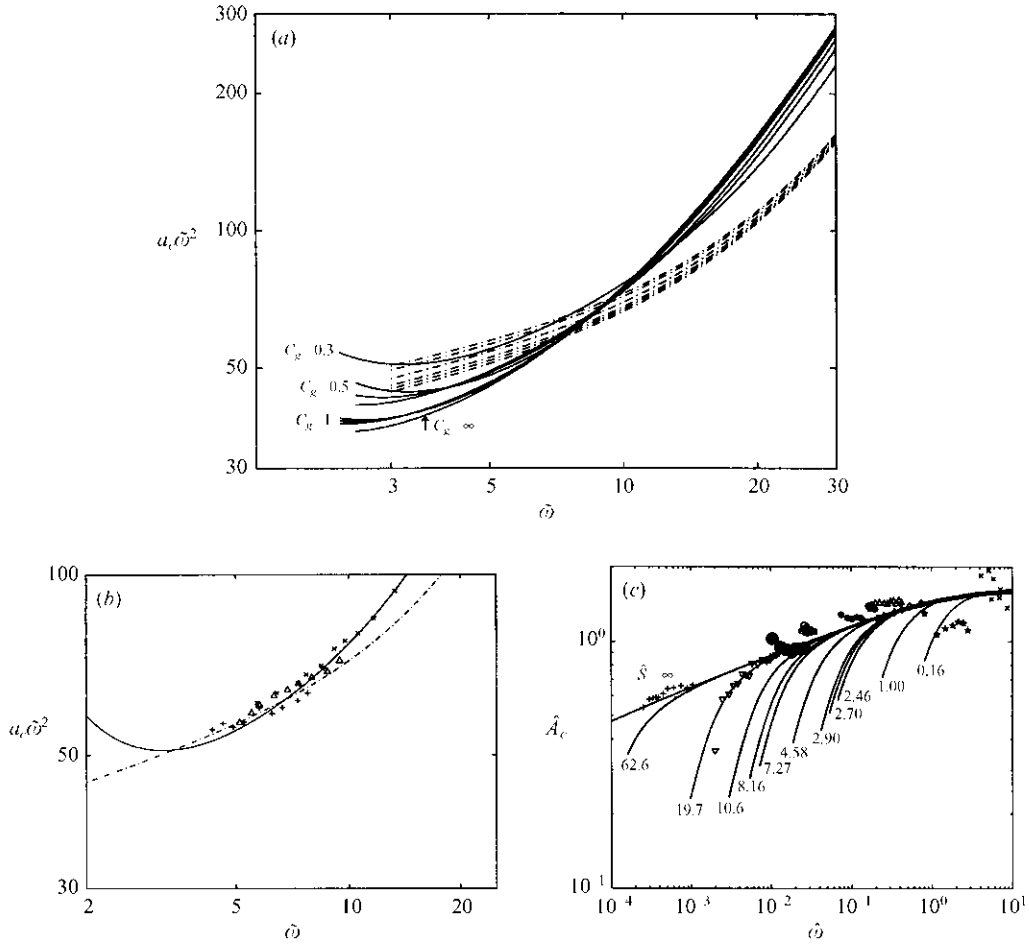


FIGURE 9. Comparison with experiments. (a) Joint plot of the right-hand sides of figure 3(c,d) and their counterparts for $C_g = 0.3$ and $S = 0.7$ (—), and the corresponding empirical approximation (6.1) (---); the values of C_g and S associated with each empirical curve are readily guessed taking into account that $a_c \hat{\omega}^2$ increases as $(1 - S)/C_g^2$ increases. (b) Comparison of the exact curves (—) and the empirical approximation (6.1) (---) for $C_g = 0.3$ and $S = 0.7$ with some experiments by Lioubashevski *et al.* (1997), see table 1. (c) A plot of some of the curves in figure 6(a) and some experimental results (see table 2).

compared with the container depth. The parameters ρ , ν and σ vary in small ranges for these experiments, and we only give an intermediate value in each case.

7. Conclusions

We have considered the linear problem giving the instability threshold amplitude, a_c , for the appearance of Faraday waves in large-aspect-ratio containers. We have identified all distinguished limits, which are listed in §1. These results allow us to explain the shape of the curve $a_c \omega^2$ vs. ω , depending on the non-dimensional parameters C_g , which is a measure of viscous effects (compared to the combined effect of gravity and surface tension) and S , which is the ratio of surface tension to its combined effect with gravity. These curves always show the same asymptotic

behaviours for small and large frequency. A sequence of alternating harmonic sub-harmonic segments appears for small frequency, as $\omega \ll 1 - S + C_g$; the practical interest of this limit is limited because it involves a quite large forcing amplitude. As $\omega \gg C_g$ and $1 - S + S\omega/C_g \ll \omega^{3/2}C_g^{1/2}$ viscous effects dominate both gravity and surface tension and we have $a_c(\omega/C_g)^{1/2} \simeq 1.672$. Two cases can be distinguished for the intermediate part of the curve:

In the basic viscous case, considered in §2.1, C_g is at least of order unity and there is only one intermediate region, obtained as $\omega/C_g \sim 1$. As a practical recipe for this limit, we have found in §6.1 that as $C_g > 0.5$ and $\omega/C_g > 5$ (for arbitrary S) all curves $a_c\omega^2/C_g^2$ vs. ω/C_g approach that curve obtained for $C_g = \infty$. This wide validity of the highly viscous limit explained some observations by Lioubashevski *et al.* (1995).

In the nearly inviscid case, as $C_g \ll 1$, the curve (see figure 7*b,c*) shows several distinguished regions in addition to the two considered above. As $\omega \sim C_g$ and $1 - S + S\omega/C_g \gg \omega^{3/2}C_g^{1/2}$ (in figure 7*b*, $\omega_1 \lesssim \omega \lesssim \omega_2$, where $\omega_1 = 0.1$ for $S = 0, 0.5$, $\omega_1 = 0.5$ for $S = 1$, and $\omega_2 = 5$ for $S = 0$, $\omega_2 = 100$ for $S = 0.5, 1$), viscous effects are weak except in boundary layers and a_c can be approximated in closed form. As $1 - S + S\omega/C_g \sim \omega^{3/2}C_g^{1/2}$ viscous effects cannot be neglected, even in a first approximation, because they are of the same order as the combined effect of gravity and surface tension; this corresponds to the transition from small to dominant viscous effects, and yield the change in slope at $\omega \sim \omega_2$ in figure 7(*b*). If $1 - S \gg C_g$ ($S = 0$ and 0.5 in figure 7*b*) there are no additional regions but if $1 - S = O(C_g)$ ($S = 1$ in figure 7*b*) there is an additional viscous region, as $\omega \sim C_g$ ($\omega \sim \omega_1$, in figure 7*b*) where the eigenfunction at threshold exhibits a long wavelength (compared to depth), which is intermediate between the nearly inviscid region and the harmonic sub-harmonic sequence. Most experiments in the literature for small C_g correspond to the short-wave part of the curve and were compared in figure 9(*c*) with the results obtained in §2.2. We have elucidated the roles of gravity and surface tension in each experiment.

In addition we have thoroughly checked two approximations in the literature, introduced by Kumar (1996) and Cerda & Tirapegui (1998), which together describe reasonably well the threshold acceleration for all values of the parameters. The former yields good results on the first resonance tongue, in most of the curve $a_c\omega^2$ vs. ω , except at small ω . And the latter applies at small frequency, so that the scope of both approximations overlaps and covers the whole curve.

The results above show that C_g and S are useful parameters for the description and understanding of the several regimes. We showed that there is a variety of essentially different regimes, some of which have not been explored experimentally. We have tried to obtain a complete description of all regimes and the scope of each. We hope this will help as a prerequisite to understanding weakly nonlinear dynamics of Faraday waves, which is a major open problem.

This research was partially supported by DGI and NASA, under Grants BFM2001-2363 and NAG3-2152. The authors are indebted to Dr Carlos Martel for some useful discussions.

Appendix. Numerical calculation of the marginal instability curves

For the sake of brevity we only give complete expressions for the basic limit considered in §2.1.1, and for convenience we consider the non-dimensional equations (2.3)–(2.6). The Floquet exponents are denoted as $\tilde{\lambda}$ and defined such that there

is a non-zero solution of (2.3) (2.6) such that $(W(\tilde{t}), \tilde{P}(\tilde{t}), \tilde{F}(\tilde{t})) \exp(-\tilde{\lambda}\tilde{t})$ is periodic, of period $2\pi/\tilde{\omega}$. The Fourier expansion of this periodic solution will converge exponentially. Accordingly, as in Kumar & Tuckerman (1994), if the expansion

$$(W(\tilde{t}), \tilde{P}(\tilde{t}), \tilde{F}(\tilde{t})) = \exp(\tilde{\lambda}\tilde{t}) \sum_{n=-\infty}^{n=\infty} (W_n, \tilde{P}_n, \tilde{F}_n) \exp(in\tilde{\omega}\tilde{t}) \quad (\text{A } 1)$$

is substituted into (1.9) (1.11) then several equations and boundary conditions result that allow a unique determination of W_n and \tilde{P}_n in terms of \tilde{F}_n . A further substitution into (1.12) yields

$$2A_n \tilde{F}_n = a\tilde{\omega}^2 (\tilde{F}_{n-1} + \tilde{F}_{n+1}), \quad (\text{A } 2)$$

where

$$A_n = \left. \begin{aligned} & \frac{[(q_n^2 + k^2)^2 + 4k^4]q_n - [(q_n^2 + k^2)^2 + 4q_n^2 k^2]k \tanh q_n \tanh k}{k(q_n \tanh k - k \tanh q_n)} \\ & - \frac{4q_n k (q_n^2 + k^2)}{q_n \cosh q_n \sinh k - k \sinh q_n \cosh k} + \frac{1 - S + Sk^2}{C_g^2}, \\ & q_n = (k^2 + \tilde{\lambda} + in\tilde{\omega})^{1/2}, \end{aligned} \right\} \quad (\text{A } 3)$$

if $\tilde{\lambda} + in\tilde{\omega} \neq 0$, and $A_0 = (1 - S + Sk^2)/C_g^2$ if $\tilde{\lambda} = 0$. Here we are assuming that the real and imaginary parts of the Floquet exponent satisfy $\text{Re}\tilde{\lambda} + k^2 \geq 0$ and $0 \leq \text{Im}\tilde{\lambda} \leq \tilde{\omega}/2$. Now, the Floquet exponents are readily calculated by imposing that the system (A 2) has a non-trivial solution, i.e. after truncation, by imposing that the associated tridiagonal matrix is singular. This condition can be written in terms of a continued fraction (Chen & Vifials 1997; Miles 1999). But that condition is also imposed quite effectively by solving iteratively the tridiagonal system (A 2) as follows. Split the system (A 2) into the sub-systems corresponding to n positive and negative, and the equation corresponding to $n = 0$, and rewrite these three problems as

$$2A_{\pm n} f_{n-1}^{\pm} = a\tilde{\omega}^2 (1 + f_{n-1}^{\pm} f_n^{\pm}) \quad \text{if } n \geq 1, \quad (\text{A } 4)$$

$$2A_0 = a\tilde{\omega}^2 (f_0^+ + f_0^-), \quad (\text{A } 5)$$

in terms of the new variables

$$f_n^{\pm} = \tilde{F}_{\pm(n+1)} / \tilde{F}_{\pm n}. \quad (\text{A } 6)$$

Since $A_N = -\tilde{\omega}^2 N^2 / (k \tanh k) + O(N) \rightarrow \infty$ as $n \rightarrow \pm\infty$, the expression

$$f_N^{\pm} = a\tilde{\omega}^2 / (2A_{\pm(N+1)}), \quad (\text{A } 7)$$

is exact up to a factor $1 + O(|f_N^{\pm}|^2)$ as $N \rightarrow \infty$. Here we are disregarding the spurious behaviour $f_N^{\pm} \sim 2A_{\pm N} / (\tilde{\omega}^2 a)$. Now, $f_1^{\pm}, \dots, f_N^{\pm}$ are uniquely determined by (A 4) and (A 7). And substitution of f_0^{\pm} into (A 5) provides the *characteristic equation* to calculate the Floquet exponent $\tilde{\lambda}$. The system (A 4) is further simplified in two cases

$$f_n^- = f_n^- \quad \text{if } \tilde{\lambda} = 0, \quad f_{n+1}^- = f_n^+ \quad \text{and} \quad |f_0^-| = 1 \quad \text{if } \tilde{\lambda} = i\tilde{\omega}/2, \quad (\text{A } 8)$$

as is readily seen.

For convenience we consider in particular a two-term truncation in the sub-harmonic case. From (A 5), (A 7) and (A 8), we obtain $2A_0 = a\tilde{\omega}^2 (f_0^+ + f_0^-)$, $f_0^+ = a\tilde{\omega}^2 / (2A_1)$ and $|f_0^-| = 1$, which lead to the following approximation of the threshold

amplitude:

$$a_c^2 \tilde{\omega}^4 = 2[A_0 A_1 + \text{c.c.} + |A_1|^2 - \sqrt{(A_0 A_1 + \text{c.c.} + |A_1|^2)^2 - 4|A_0|^2 |A_1|^2}], \quad (\text{A } 9)$$

where A_0 and A_1 are given by (A 3), with $\tilde{\lambda} = i\tilde{\omega}/2$. This approximation coincides with that by Kumar (1996) modulo notation differences.

The problems (2.11)–(2.13), (2.29)–(2.32) and (2.29)–(2.31), (2.35) are solved in a completely similar way. Equations (A 4)–(A 8) remain unchanged, while (A 2) must be replaced by the following expressions, which are obtained by substituting the scalings (2.2), (2.10) and (2.34) into (A 1)–(A 2), (A 4)–(A 7) and neglecting higher-order terms. For (2.11)–(2.13) we have

$$A_n = \tilde{q}_n^5 / [(\gamma + 1)\tilde{k}^2(\tilde{q}_n - \tanh \tilde{q}_n)] + \gamma + (\gamma + 1)\tilde{k}^2, \quad (\text{A } 10)$$

where $\tilde{q}_n = (\tilde{\lambda} + i n \tilde{\omega})^{1/2}$; for (2.29)–(2.32) we obtain

$$A_n = (\hat{q}_n^2 + \hat{k}^2)^2 / \hat{k} - 4\hat{k}^2 \hat{q}_n, \quad \hat{q}_n = (\hat{k}^2 + \hat{\lambda} + i n \hat{\omega})^{1/2}, \quad (\text{A } 11)$$

and for (2.29)–(2.31) and (2.35) we obtain

$$A_n = (\hat{q}_n^2 + \hat{k}^2)^2 / \hat{k} - 4\hat{k}^2 \hat{q}_n + (1 + \hat{S})^{-3} \hat{\omega}^{-3/2} + \hat{S} \hat{k}^2 (1 + \hat{S})^{-1} \hat{\omega}^{-1/2}, \quad (\text{A } 12)$$

with \hat{q}_n as defined in (A 11).

REFERENCES

- ABRAMOWITZ, M. & STEGUN, I. A. 1972 *Handbook of Mathematical Functions*. Dover.
- BECHHOEFFER, J., EGO, V., MANNEVILLE, S. & JOHNSON, B. 1995 An experimental study of the onset of parametrically pumped surface waves in viscous fluids. *J. Fluid Mech.* **288**, 325–350.
- BENDER, C. M. & ORSZAG, A. O. 1978 *Advanced Mathematical Methods for Scientists and Engineers*. McGraw-Hill.
- BEYER, J. & FRIEDRICH, R. 1995 Faraday instability: linear analysis for viscous fluids. *Phys. Rev. E* **51**, 1162–1168.
- CERDA, E. & TIRAPUGUI, E. 1998 Faraday's instability in viscous fluid. *J. Fluid Mech.* **368**, 195–228.
- CHEN, P. & VIÑALS, J. 1997 Pattern selection in Faraday waves. *Phys. Rev. Lett.* **79**, 2670–2673.
- CHRISTIANSEN, B., ALSTROM, P. & LEVINSSEN, M. T. 1995 Dissipation and ordering in capillary waves at high aspect ratios. *J. Fluid Mech.* **291**, 323–341.
- DOUADY, S. 1990 Experimental study of the Faraday instability. *J. Fluid Mech.* **221**, 383–409.
- EDWARDS, W. S. & FAUVE, S. 1994 Patterns and quasipatterns in the Faraday experiment. *J. Fluid Mech.* **278**, 123–148.
- FARADAY, M. 1831 On the forms and states assumed by fluids in contact with vibrating elastic surfaces. *Phil. Trans. R. Soc. Lond.* **121**, 319–340.
- FAUVE, S. 1995 Parametric instabilities, in *Dynamics of Nonlinear and Disordered Systems* (ed. G. Martínez-Mekler & T. H. Seligman), pp. 67–115. World Scientific.
- HENDERSON, D. M. & MILES, J. W. 1990 Single mode Faraday waves in small cylinders. *J. Fluid Mech.* **213**, 95–109.
- HENDERSON, D. M. & MILES, J. W. 1994 Surface-wave damping in a circular cylinder with a fixed contact line. *J. Fluid Mech.* **275**, 285–299.
- HOCKING, L. M. 1987 The damping of capillary gravity waves at a rigid boundary. *J. Fluid Mech.* **179**, 253–266.
- HOFFMANN, F. M. & WOLLE, G. H. 1974 Excitation of parametric instabilities in statically stable and unstable fluid interfaces. *J. Appl. Phys.* **45**, 3859–3863.
- HOWELL, D., HEATH, T., MCKENNA, C., HWANG, W. & SCHATZ, M. F. 2000 Measurements of surface-wave damping in a container. *Phys. Fluids* **12**, 322–326.
- JIANG, L., TING, C.-L., PERLIN, M. & SCHULTZ, W. W. 1996 Moderate and steep Faraday waves: instabilities, modulation and temporal asymmetries. *J. Fluid Mech.* **329**, 275–307.

- KNOBLOCH, E., MARTEL, C. & VEGA, J. M. 2002 Coupled mean flow-amplitude equations for nearly inviscid parametrically driven surface waves. *Ann. NY Acad. Sci.* **974**, to appear.
- KUDROLLI, A. & GOLLUB, J. P. 1996 Patterns and spatio-temporal chaos in parametrically forced surface waves: a systematic survey at large aspect ratio. *Physica D* **97**, 133–154.
- KUMAR, K. 1996 Linear theory of Faraday instability in viscous fluids. *Proc. R. Soc. Lond. A* **452**, 1113–1126.
- KUMAR, K. & TUCKERMAN, L. S. 1994 Parametric instability of the interface between two fluids. *J. Fluid Mech.* **279**, 49–68.
- LIUBASHEVSKI, O., FINEBERG, J. & TUCKERMAN, L. S. 1997 Scaling of the transition to parametrically driven surface waves in highly dissipative systems. *Phys. Rev. E* **55**, R3832–R3835.
- MARTEL, C. & KNOBLOCH, E. 1997 Damping of nearly-inviscid water waves. *Phys. Rev. E* **56**, 5544–5548.
- MARTEL, C., NICOLÁS, J. A. & VEGA, J. M. 1998 Surface-wave damping in a brimful circular cylinder. *J. Fluid Mech.* **360**, 213–228; and Corrigendum, **373**, 379.
- MILES, J. W. 1999 On Faraday resonance of a viscous fluid. *J. Fluid Mech.* **395**, 321–325.
- MILES, J. & HENDERSON, D. 1990 Parametrically forced surface waves. *Annu. Rev. Fluid Mech.* **22**, 143–165.
- MILNER, S. T. 1991 Square patterns and secondary instabilities in driven capillary waves. *J. Fluid Mech.* **225**, 81–100.
- MÜLLER, H. W., WITTMER, H., WAGNER, C., ALBERS, J. & KNORR, K. 1997 Analytic stability theory for Faraday waves and the observation of the harmonic surface response. *Phys. Rev. Lett.* **78**, 2357–2360.
- WASOW, W. 1987 *Asymptotic Expansions for Ordinary Differential Equations*. Dover.
- WERNET, A., WAGNER, C., PAPATHANASSIOU, D., MÜLLER, H. W. & KNORR, K. 2001 Amplitude measurements of Faraday waves. *Phys. Rev. E* **63**, 036305.1–9.
- WOLF, G. H. 1970 Dynamic stabilization of the interchange instability of a liquid–gas interface. *Phys. Rev. Lett.* **24**, 444–446.